Japanese Journal of Structural Geology, No. 47, 37-48, 2003

Article

Stress distribution and seismic faulting in the Nepal Himalaya : insights from finite element modeling

Md. Mahmudul Alam* and Daigoro Hayashi*

Abstract : In this study we use 2D finite element modeling to predict stress distribution and fault development during N-S shorting in the Himalayas. The direction of maximum compressive stress (σ_1) is horizontal within the shallow levels of both models. Variation in the displacement boundary conditions results in changes of principal stress directions in the deep crust while stresses in the shallow crust remain unchanged.

Mohr-Coulomb failure is observed along near-surface sections of the Siwalik, Tethys and Granitic basement layers, with minor failure near the surface of the MBT, MCT and STDS. Failure does not occur due to hydrostatic conditions in the deeper part of the Higher Himalaya, the Lesser Himalaya or the Granitic basement layer, despite changing the rheology of rock layers. Focal mechanism solutions of earthquakes in the Himalayan region suggest the existence of thrust faults stretching along EW with one plane dipping gently north beneath the Himalaya. The simulations predict a similar distribution of thrust faults along the upper part of the Himalaya.

Key words : *Finite Element Method (FEM), Mohr-Coulomb failure, Main Boundary Thrust (MBT), Main Central Thrust (MCT), South Tibetan Detachment System (STDS), Focal mechanism.*

Introduction

Finite element modeling is an effective tool for studying tectonic deformation in the crust. The Himalayan mountain chain formed following collision of the Indian and Eurasian plates (Fig. 1 ; Dewey and Bird, 1970 ; Windley, 1984, 1995). Following Eocene collision of the two continents, further convergence and crustal shortening was taken up in major intercontinental subduction which led to the formation of the Himalayan chain (Pecher, 1989).

The continent-continent collision model for the uplift of the Tibetan Plateau has been modeled numerically by England and others (England and McKenzie, 1982, 1983 ; England and Houseman 1985, 1986). In these studies, they assumed the Indian and Asian crusts to be an incompressible non-Newtonian fluid and the collision was analysed in 3-dimension by means of a thin viscous sheet analysis and had the intention of explaining the structure of the interior of the Asian continent.

The large negative gravity anomalies over the Ganga Basin and the Himalaya are reproduced by a model where the Indian crust underthrusts Himalaya at shallow angles of $15° \pm 5°$ along several thrust zones (Indus Suture Zone, MCT and MBT ; Warsi and Molnar, 1977). In this model the Himalayan region is isostatically uncompensated and crustal shortening of 300 to 400 km is calculated to have occurred across the orogenic belt.

Hayashi (1987, 1992) numerically simulated the uplift of the Tibetan plateau and the Himalayas by finite element modeling, assuming that the northerly migration of the Indian plate deforms the overlying Asian continental crust which behaves as an incompressible Newtonian fluid above the rigid upper mantle. In these models, the upper mantle lithosphere is a rigid body for the first approximation and the deformable crust overlies the upper mantle. The deforma-

Received 8 April 2002 ; accepted 16 January 2003
* Department of Physics and Earth Sciences, University of the Ryukyus, Okinawa, Japan

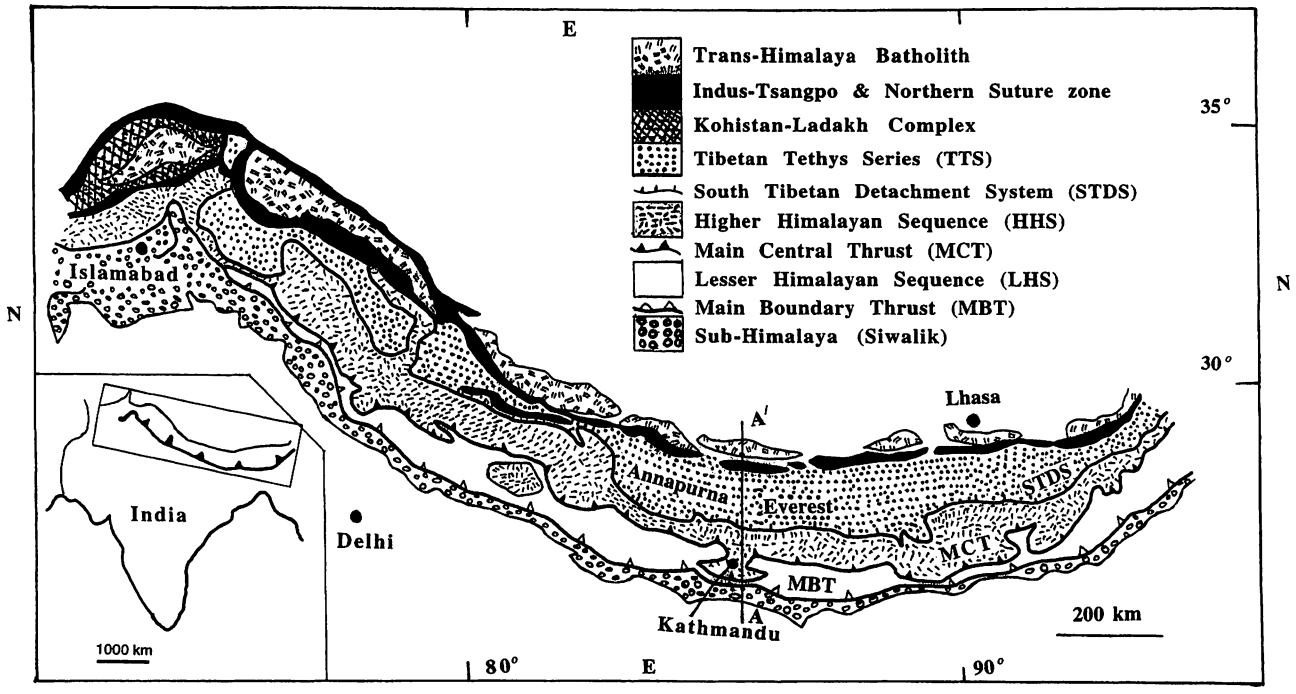

Fig. 1 Simplified geologic map of the Himalaya showing the major tectonostratigraphic divisions. Modified from Gansser (1964), Le Fort (1975), Barnicot and Treloar (1997), Parrish and Hodges (1997), and Kaneko (1997).

tion of the crust is then expected to form plateaus and mountain ranges. Under such an assumption, isostatic readjustment becomes impossible and the calculated values of surface uplift tend to be overestimated. Further, the rigid plate assumption prohibits simulation for a period longer than 0.1 Ma.

The aim of this study is to simulate the stress distribution and patterns of fault development in the Nepal Himalaya by means of two-dimensional plane strain FEM. In the FEM analysis, it is assumed that geological material is homogeneous and elastic, although it is likely that crustal rocks are visco-elastic (Makel and Walters, 1993 ; Bott and Stern, 1992 ; Ghose et al., 1990). This assumption is simple, but the modeling is instructive and contributes to our understanding of the Himalayas.

Calculated principal stresses and failure elements are used to identify the fault pattern. We focus our investigation on the following three points : (i) intensity and direction of principal stresses along the Nepal Himalaya under various boundary conditions, (ii) development of faults, and (iii) comparison of the simulated stress distribution with focal mechanism solutions from the Himalaya region.

Geological Setting

The Himalayan mountain chain is divided longitudinally by principal thrusts into four tectonic zones ; the Sub-Himalaya (SH), the Lesser Himalaya (LH), the Higher Himalaya (HH), and the Tethys Himalaya (Gansser, 1964). The principal thrusts are the MBT, MCT and STDS (Fig. 1).

1. Sub Himalaya (Siwalik)

Forming the southernmost belt of the Himalayan range, the Siwaliks are the lowest and narrowest range in the Himalayan system, with an average elevation of about 900–1200 m and, a width of as little as 16 km. The Sub-Himalayan zone is bounded by the MBT to the north along the southern foot of the Mahabharat Range and the Main Frontal Thrust (MFT) to the south at the southern edge of the Siwalik (Churia) Group (Kizaki, 1994).

2. Lesser Himalaya

The Lesser Himalaya has been variously named the Midland meta-sediments (Arita, 1983) and Lesser Himalayan Sequence (Kaneko, 1995,

1997). Lying between the HH region in the north and the Siwaliks to the south, the LH region forms the intermediate zone of the Himalayan mountain chain (Sakai, 1985). Lower than the HH, this region has an average altitude of 3700–4500 m.

3. Higher Himalaya

The Higher Himalaya is bounded to the south by the MCT, and to the north by the STDS. The STDS is a series of normal faults on the northern flank of the Himalaya, and forms the contact between Tibetan Tethys sediment and underlying Higher Himalayan Sequence (Hashimoto et al., 1973 ; Burg and Chen, 1984 ; Burchfiel et al., 1992). The HH has been previously named the Himalayan Gneiss (Arita, 1983), Higher Himalayan Sequence (Kaneko, 1994, 1995). The Higher Himalayan belt forms the backbone in the Himalayan system. With an average elevation of about 6100 m, the HH dominates the northern frontiers of India and the entire northern boundary of Nepal.

4. Tethys Himalaya

The Tethys Himalaya is seperated from the HH by STDS to the north. In the Tibetan Himalayan zone, the Palaeozoic to early Cenozoic Tethys sediments are distributed along the southern most margin of the Tibetan Tethys basin, such as the Sagarmatha region, the Langu-Manang basin, the Saipal - Amlang basin, the Spiti basin and the Kashimir basin which is underlain by granite (Kizaki, 1994).

Finite Element Modeling

In our modeling, the significant parameters are the rock properties including cohesion and angle of internal friction. Cross sections of two models are shown in Figs. 2–3. All simulations were conducted using the rock properties and boundary conditions shown in Table 1 and 2, and Figs. 4–5. In this simulation, we investigated how stress orientation and fault pattern are influenced by rock properties and boundary conditions of two-dimensional FEM. First we conducted test calculations using a standard model in order to determine the range of the key parameters, such as Young's modulus, Poisson's ratio, strength and angle of internal friction of rock formations. Then taking into account the results of the test, we simulated the principal stresses and failure blocks under most reasonable boundary conditions.

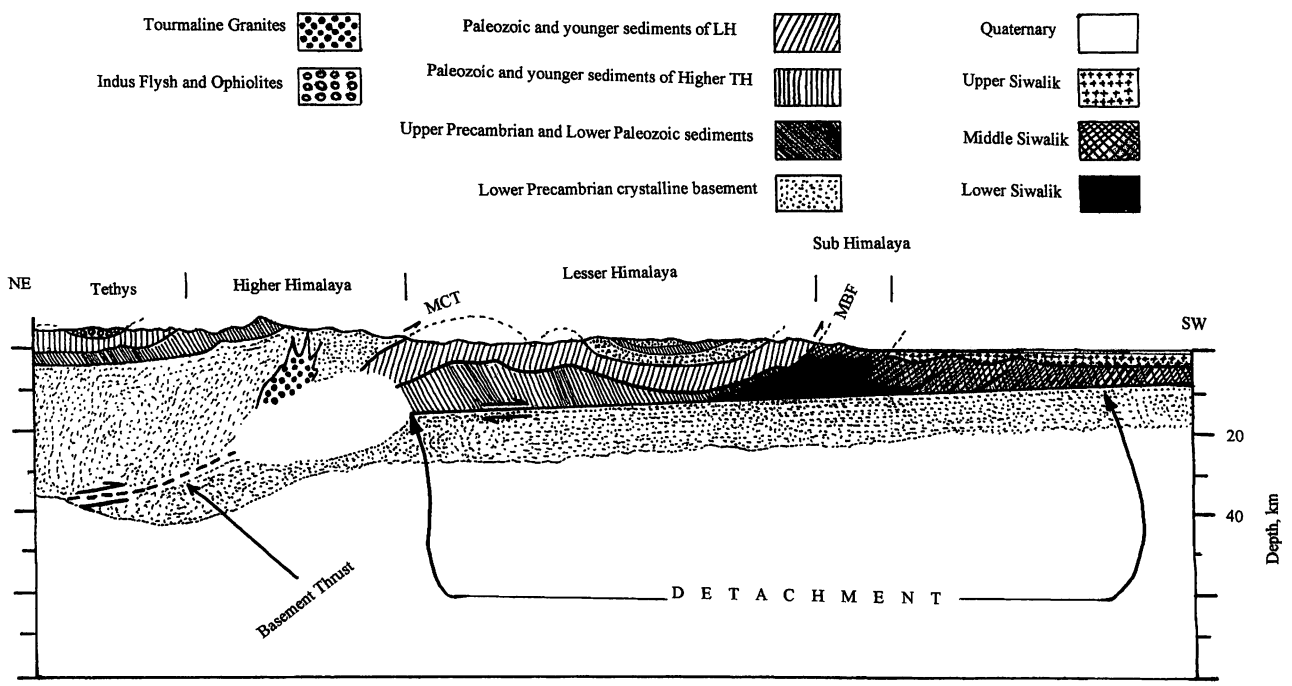

Fig. 2 Cross section (A'-A in Fig. 1) of the central Himalaya. Modified from Seeber et al. (1980) and Gansser (1964). MCT : Main central thrust, MBF : Main boundary front.

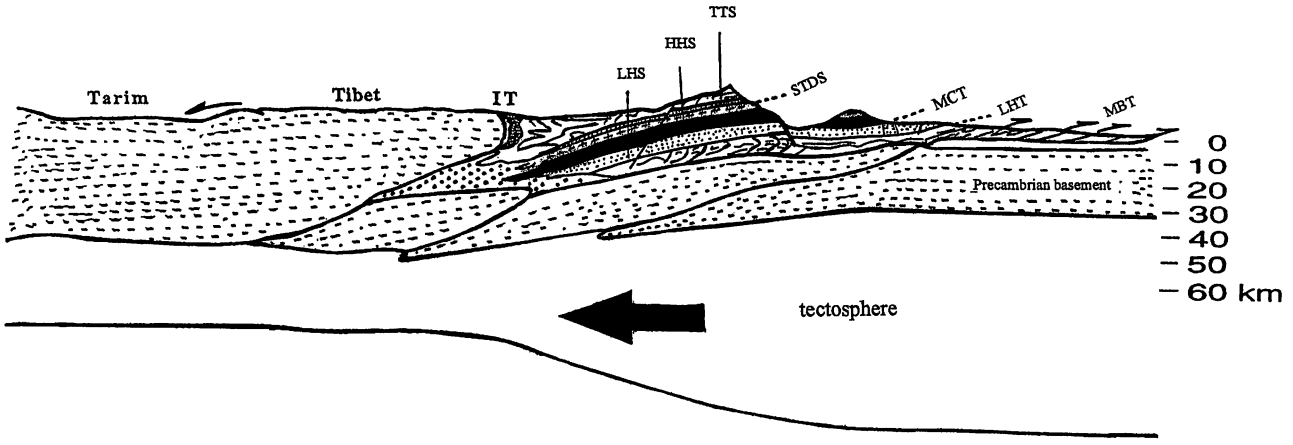

Fig. 3 Geological cross section (A-A′ in Fig. 1) of the Himalayan Metamorphic belt in central Nepal. Modified from Kaneko (1997). LHT : Lesser Himalayan thrust, STDS : South Tibetan detachment system, HHS : Higher Himalayan sequence, LHS : Lesser Himalayan sequence, IT : Indus suture, TTS : Tibetan Tethys sequence.

Methods

1. Convergence rate

The Indian plate is currently moving northward at a rate of 50 mm/yr and is underthrusting Tibet (Thakur et al., 2000). Of the total convergence, ~20 mm/yr is accommodated across the Himalaya (Bilham et al., 1997 ; Lave and Avouac, 1998) and the remaining convergence is taken up farther north (Peltzer and Saucie, 1996 ; Yeats and Thakur, 1998). Lyan-Caen and Molnar (1985) suggested a thrusting rate of between 10 and 15 mm/yr during the last 15 to 20 Ma. An estimated 3-400 km of shortening has occurred in the Himalaya (Gansser, 1966 ; Warsi and Molnar, 1977) and assuming that underthrusting began in the Oligocene or late Eocene (Gansser, 1964), the average rate of shortening is about 10 mm/yr. This rate is consistent with the rate of 10 to 20 mm/yr inferred by Molnar et al. (1977), and from seismic moments of earthquakes (Chen and Molnar, 1977). Over geological time scale (5 Ma) the ~20 mm/yr estimated shortening rate (Cattin and Avouace, 2000) across the range is accommodated by localized thrust faulting along the Main Himalayan Thrust (MHT). From the above discussion we may conclude that the most reasonable convergence rate is 10~20 mm/yr, on the average 15 mm/yr that is taken in our simulation.

2. Constraints of model geometry and boundary condition

We have selected two representative geological sections (Fig. 2, Seeber et al., 1979, and Fig. 3, Kaneko, 1997) across which we simulate stress distribution and fault development. Both models are between 90 to 105 km long and 20 to 25 km in depth.

The Himalayan profile, model 1 is composed of four tectonic zones ; Siwalik (sandstone, siltstone, mudstone), Lesser Himalaya (sandstone, limestone), Higher Himalaya (gneiss and granite), and Tethys Himalaya (sandstone, impure limestone). For model 2, we added a "Granitic basement layer", which is composed of gneiss and granite. The rock properties of the models are shown in Table 1 and 2.

We have used 75 m (for 5000 years at 15 mm/yr) and 375 m (for 25000 years) as the displacement imposed at the right edge of cross sections. In all models the upper surface is a free surface. The lower boundary is restricted vertically but allowed to move horizontally. The nodes at the left boundary can move only vertically (zero horizontal displacement). The node at the junction of the lower and the left boundary is fixed. Horizontal shortening of up to 75 m (or 375 m) is applied proportionally from the southern edge (75 m or 375 m) to the north (0 m) over the cross-section (Figs. 4-5).

3. Proximity to rock failure under Mohr - Coulomb criterion

Table 1 Rheology of rock units for model 1.

Tectonic unit	Including rock	Poisson's ratio	Density (kg/m^3)	Young's Modulus (GPa)	Angle of internal friction (degree)	Cohesion (MPa)
SH	Sandstone Siltstone Mudstone	0.25	2,500	40	35	18
LH	Sandstone Limestone	0.30	2,800	70	50	17
HH	Gneiss Granite	0.35	2,900	80	58	10
TH	Sandstone Impure limestone	0.25	2,600	50	45	20

Table 2 Rheology of rock units for model 2.

Tectonic unit	Including rock	Poisson's ratio	Density (kg/m^3)	Young's Modulus (GPa)	Angle of internal friction (degree)	Cohesion (MPa)
SH	Sandstone Siltstone Mudstone	0.25	2,600	40	35	18
LH	Sandstone Limestone	0.30	2,600	60	48	15
HH	Gneiss Granite	0.35	2,900	80	50	17
TH	Sandstone Impure limestone	0.25	2,600	50	45	20
Granitic Layer	Gneiss Granite	0.35	2,900	80	58	10

Mohr-Coulomb failure criterion is a condition that helps to identify the location of failure within the crust or at the surface. Since we compute a two-dimensional stress field on plane strain state, the third principal stress (σ^*) can be obtained from the equation

$$\sigma^*=\nu(\sigma_1+\sigma_2) \quad (1)$$

where ν is Poisson's ratio (Timoshenko and Goodier, 1970 ; Hayashi and Kizaki, 1972 ; Lu and Hayashi, 2001), and σ_1 and σ_2 are the principal stresses. After evaluating the values of σ_1, σ_2 and σ^* for each element, we compute which principal stresses, σ_1, σ_2, and σ^* are the maximum compressive, intermediate and minimum compressive. According to the order of magnitude and the sign, we define the new principal stresses, σ_1, σ_2 and σ_3.

The proximity to failure (P_f) is defined as the ratio of the radius of the Mohr circle (calculated stress) $\frac{\sigma_1-\sigma_3}{2}$, and the radius at failure (yield stress) $\left(\frac{\sigma_1-\sigma_3}{2}\right)_{failure}$ as follows.

$$p_f=\left(\frac{\left(\frac{\sigma_1-\sigma_3}{2}\right)}{\left(\frac{\sigma_1-\sigma_3}{2}\right)_{failure}}\right) \quad (2)$$

where $\left(\frac{\sigma_1-\sigma_3}{2}\right)_{failure}=c\cos\phi+\left(\frac{\sigma_1-\sigma_3}{2}\right)\sin\phi$, here c and ϕ are cohesive strength and angle of internal friction respectively. One can evaluate whether faulting develops in a certain element according to the value of the parameter P_f. If $P_f<1$, the stress state is within the failure envelope (i.e., no fault develops), but if $P_f\geq 1$, failure occurs.

Modeling Results

The numerical modeling of the Himalayan

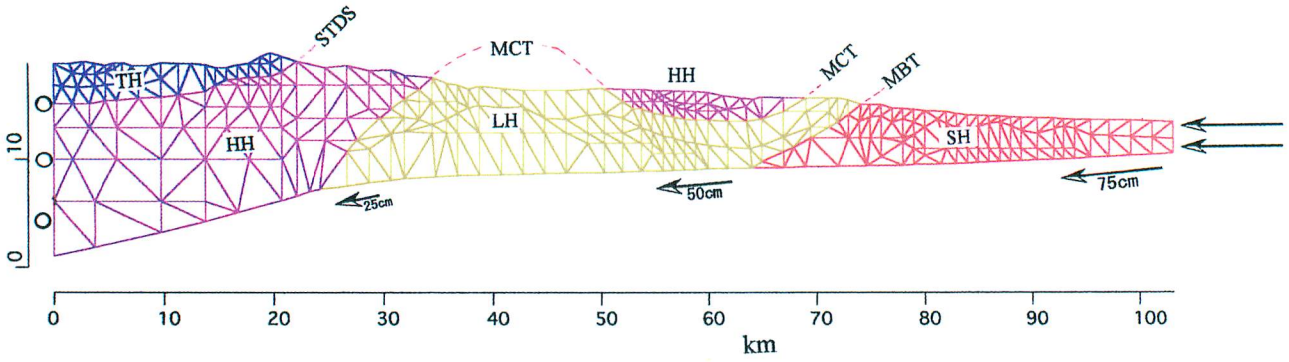

Fig. 4 Boundary conditions of Model 1. The model contains 352 nodes and 564 elements.

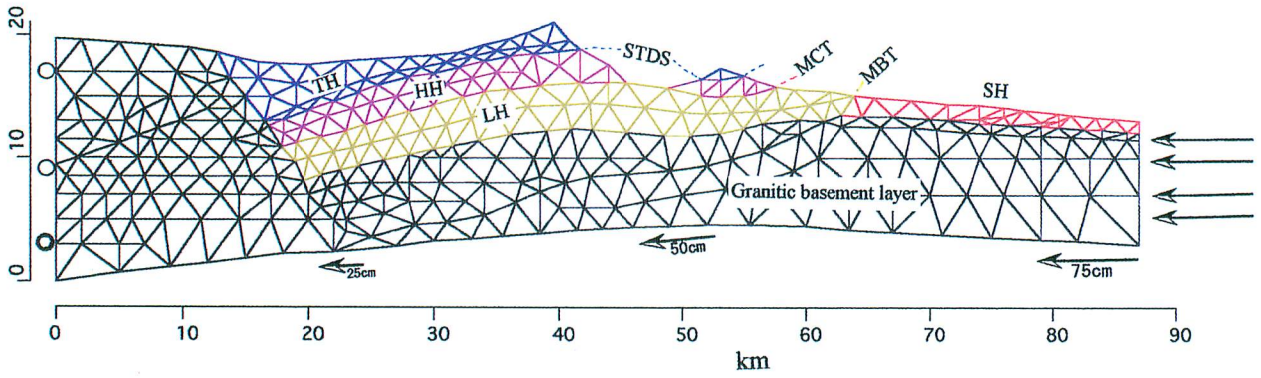

Fig. 5 Boundary conditions of Model 2. The model contains 353 nodes and 624 elements.

system has revealed two principal stress regimes, characterized by tension and compression. Stress distribution and fault patterns are controlled by two parameters ; displacement boundary conditions, and rheology. The numerical experiments show that realistic deformation of rock layers are calculated for the specific sets of displacement boundary condition (75 m/5000yr, 150 m/10000yr, 225 m/15000yr, 300 m/20000yr, and 375 m/25000yr for 15 mm/yr) and also for the values of cohesion and angle of internal friction. The occurrence Mohr-Coulomb failure depends on the values of displacement boundary condition, cohesive strength (c) and angle of internal friction (ϕ). An important advantage of numerical modeling compared to scale modeling is that the former is able to calculate the stress field at any time anywhere in the structure. Figs. 6–9 show the magnitude and orientation of principal stresses in the rock layer during progressive displacement from 75 m to 375 m displacement. σ_1 and σ_3 are the maximum and minimum compressive stresses respectively.

For both the models, maximum value of compressive σ_1 and σ_3 are 500 MPa and 360 MPa, respectively in the case of the displacement boundary condition 75 m. While maximum values of compressive σ_1 and σ_3 are 800 MPa and 600 MPa, respectively in the case of the displacement boundary condition 375 m. Maximum tensile σ_3 is 95 MPa. Directions of σ_1 are shown in Tables 3 and 4.

Discussion

1. Pattern of stress and failure in the Himalaya

Modeling result shows that in the upper part of each model, direction of σ_1 is horizontal but vertical direction is found in the deeper part

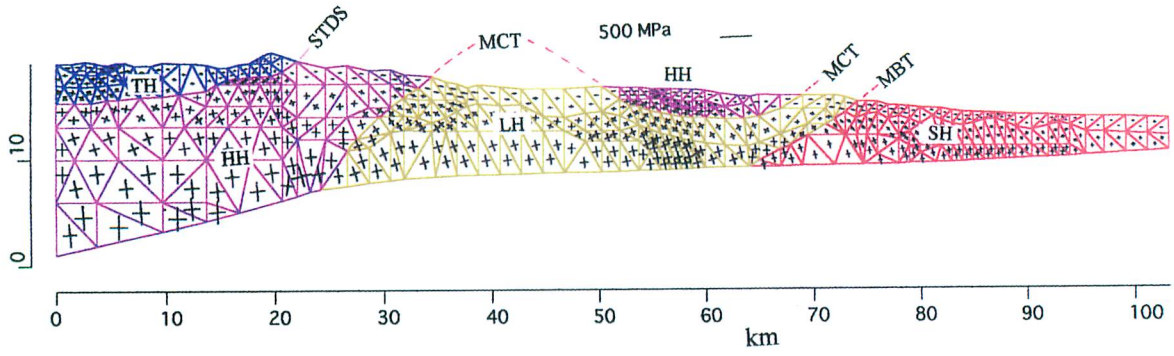

Fig. 6 Stress distribution in Model 1. 75 m displacement boundary condition is applied to the base of the model during a 5000 year interval.

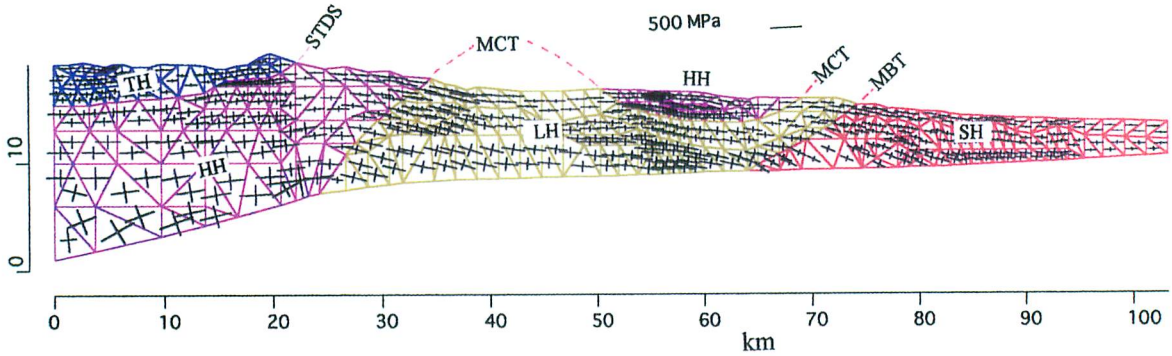

Fig. 7 Stress distribution in Model 1. 375 m displacement boundary condition is applied to the base of the model during a 25000 year interval. Red arrows indicate an extensional stress field.

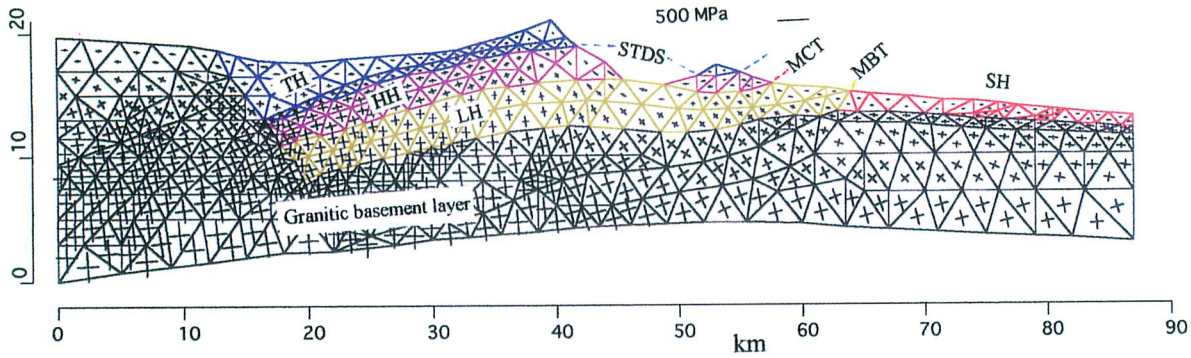

Fig. 8 Stress distribution of Model 2. 75 m displacement boundary condition is applied to the base of the model during a 5000 year interval.

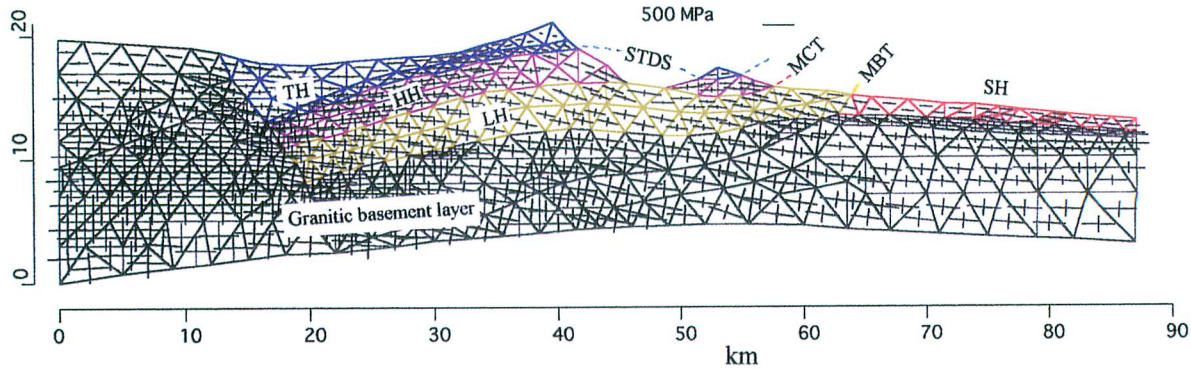

Fig. 9 Stress distribution of Model 2. 375 m displacement boundary condition is applied to the base of the model during a 25000 year interval. Red arrows indicate an extensional stress field.

Table 3 Direction of σ_1 in model 1. H : Horizontal, V : Vertical, Hydr : Hydrostatic, Sub H : Sub-Horizontal.

Convergence displacement	Depth	SH	LH	HH	TH
75 m	Upper	H	H	H	H
	Middle	Hydr	Sub H	Hydr	H
	Lower	V	V	V	Hydr
375 m	Upper	H	H	H	H
	Middle	H	H	H	H
	Lower	H	H	Hydr	H

Table 4 Direction of σ^1 in model 2. H : Horizontal, V : Vertical, Hydr : Hydrostatic, GL : Granitic Basement Layer.

Displacement	Region	SH	LH	HH	TH	GL
75 m	Upper	H	H	H	H	H
	Middle	Hydr	Hydr	H	H	Hydr
	Lower	V	V	Hydr	H	V
375 m	Upper	H	H	H	H	H
	Middle	H	H	H	H	H
	Lower	H	Hydr	Hydr	H	H

under the boundary condition 75 m. Under the displacement boundary condition 375 m, in most of the regions of all the models, σ_1 is horizontally directed. The simulation shows that the principal stresses are stronger in the deeper part than the shallower one. Principal stresses are compressive along all the region but some elements on the shallower region of the HH (red arrows in Figs. 7 and 9) showing tensile stress (less than 100 MPa) field.

The values of cohesive strength (c) and angle of internal friction (ϕ) are shown in Tables 1 and 2. For displacement of less than 75 m, no failure occurs in any of the models. As displacement increases to 225 m failure occur at the shallow levels. At 375 m of displacement, failure occurs in the shallow levels of all the models, and most of the failure occurs at the SH, the Tethys Himalaya and the Granitic basement layer (Figs. 10–11). Also some failure occurs along the upper boundaries of MBT, MCT, and STDS (Figs. 10–11). Even after varying controlling parameters, we did not obtain failure in the deeper parts of the HH, LH and Granitic basement layer. This is due to hydrostatic conditions in these areas. The elements of the greatest proximity to failure occur along surface and number of the element decreases progressively with depth due to the material properties of rock formation. After 375 m of convergence, the uppermost parts of both the models are failed over the entire length (Figs. 10–11). As the failure proximity ratio varies within a layer, the lower parts of each layer are out of failure but upper parts are under failure (Figs. 10–11).

2. Comparison of faulting pattern with focal mechanism data

The Nepal Himalaya consists of nappes and thrust blocks that are thrust southward onto the Indian shield (Gansser, 1964 ; LeFort, 1975 ; Pecher, 1989 ; Valdia, 1980 a, 1980 b, 1981 ; Baranowski et al., 1984). The Indian shield is warped under the Himalaya and underthrusts the LH to a gentle northerly or northeasterly dipping thrust fault (Seeber et al., 1981). Lyon-Caen and Molnar (1983) reached the same conclusion from a study of gravity anomalies over the Himalaya, assuming that the Indian plate is flexed down by the weight of the Himalayan range thrust on top of it.

Focal mechanisms of shallow depth earthquakes show compressive stress pattern along

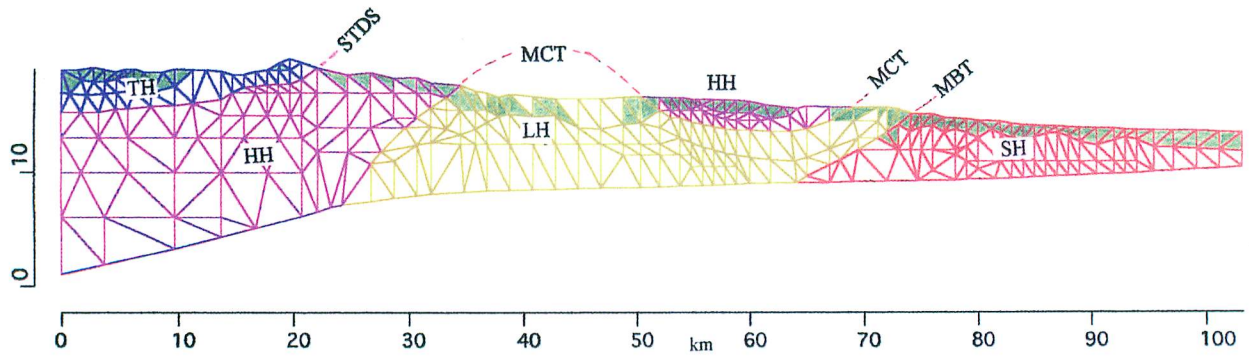

Fig. 10 Failure elements of Model 1. Green blocks indicate failure.

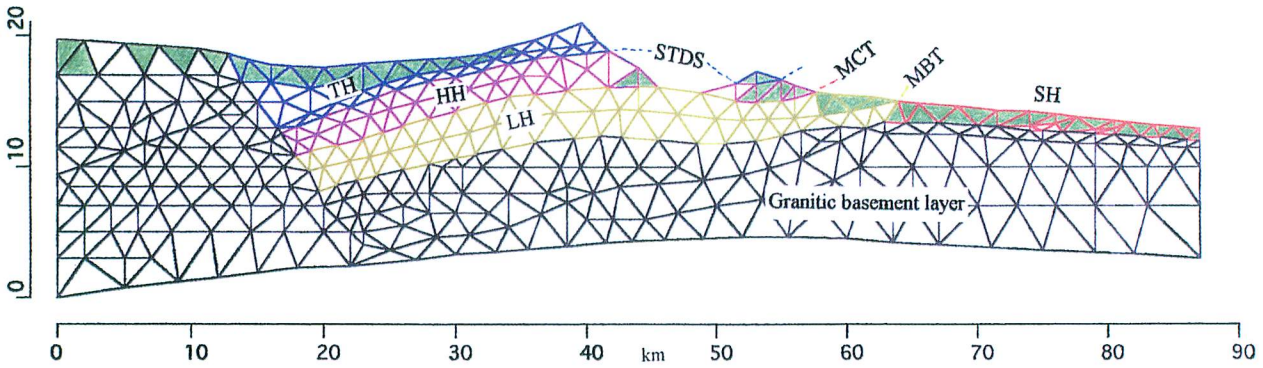

Fig. 11 Failure elements of Model 2. Green blocks indicate failure.

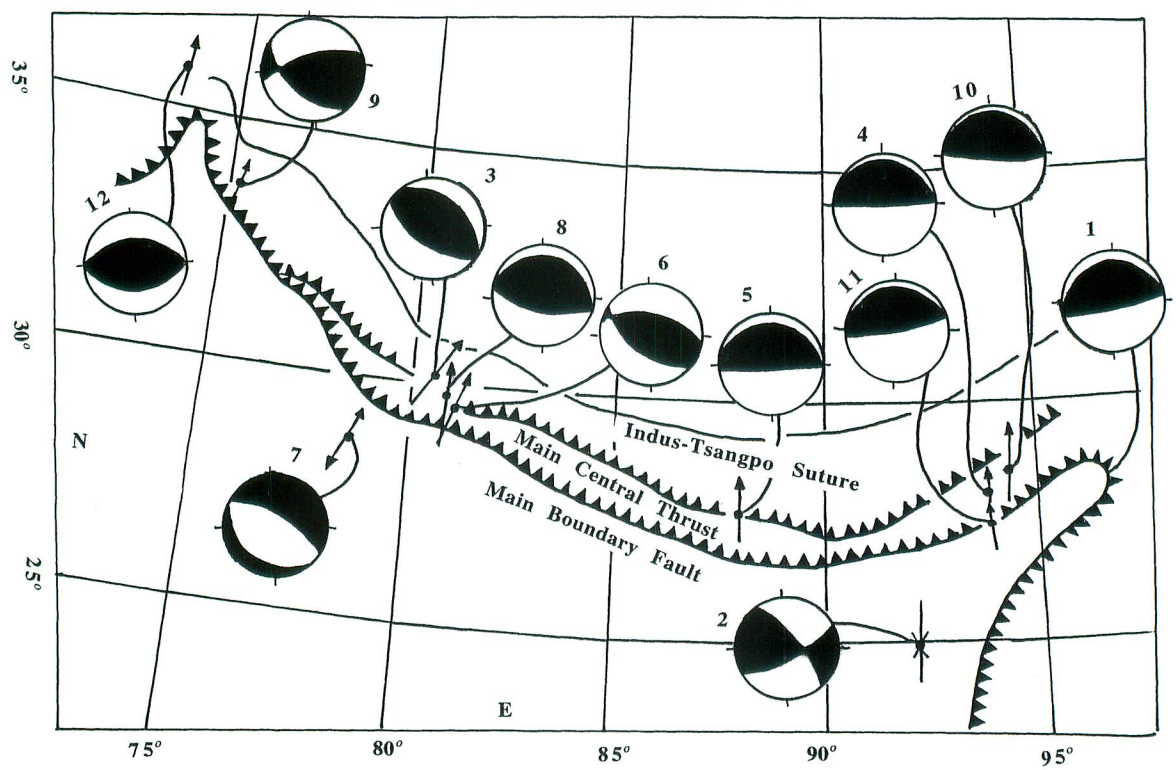

Fig. 12 Focal mechanism solutions. Single arrows show presumed direction on underthrusting. Opposing arrows for event 2 show approximate direction of maximum compression and diverging arrows for event 7 show approximate direction of least compression. Circles show lower hemisphere plots of focal sphere - dark areas represent quadrant with compressional first arrivals (Molnar et al., 1977).

the Himalayan region. Several published studies of focal mechanism solutions of earthquakes in the Himalayan region give the same general pattern of thrust faulting, with one plane dipping gently beneath the Himalaya (Fitch, 1970 ; Ichikawa et al., 1972 ; Molnar et al., 1973 ; Rastogi et al., 1974 ; Banghar, 1974 ; Tandon and Srivastava, 1975 ; Armbruster et al., 1978 ; Chen and Molnar, 1977 ; Chandra, 1978 ; Baranowski, et al., 1984 ; Fig. 12). The present study also shows the same pattern of thrust faulting in the shallower region of the Himalaya, whatever the boundary condition might be.

3. Limitation of our analysis

(1) We assume that geological body is elastic, though the body in nature has to be elastoplastic when we consider about faulting.

(2) Each tectonic zone is composed of several rock layers. The composite tectonic zone is assumed to have the average physical properties of several rock layers, while each rock layer has distinct physical properties. This estimation of average properties of tectonic zone is not fully justified, though we believe this is the better way at present

Conclusion

The results of our finite element models of the Nepal Himalaya are as follows.

(1) Variation of the displacement boundary condition results in changes of the direction of principal stresses in the deeper part of the crust while principal stresses in shallower levels remain unchanged.

(2) Stress is most likely compressive for all the models, although greater displacement produces tensile stresses (less than 100 MPa) in shallow levels of the crust.

(3) Mohr-Coulomb failure is observed along the shallower part of Siwalik, Tethys, Granitic basement layer, and near the surface of MBT, MCT and STDS.

(4) Despite changing simulation parameters, failure did not occur in the deeper part of the HH, LH and Granitic basement layer. This is due to the hydrostatic state condition.

(5) Focal mechanism solutions of earthquakes in the Himalayan region reveal the existence of thrust faults that dip gently north. The simulation predicts the same distribution of thrust faults along the upper part of the models as shown by focal mechanism solutions.

Acknowledgments

We would like to express gratitude to the Ministry of Education, Science and Culture, Japan (MONBUSHO) for financial support during the study. We thank Aaron Stallard of university of Canterbury, New Zealand for critical review.

References

Arita, K., 1983, Origin of the inverted metamorphism of the lower Himalaya, central Nepal. *Tectonophysics,* **95**, 43-60.

Armbraster, J., Seeber, L. and Jacob, K.H., 1978, The northwestern termination of the Himalayan mountain front : Active tectonics from micro earthquakes. *J. Geophys. Res.* **83**, 269-282.

Banghar, A.R., 1974, Focal mechanisms of earthquakes in China, Mongolia, Russia, Nepal, Pakistan, and Afghanistan. *Earthq. Notes,* **45**, 1-11.

Baranowski, J., Armbruster, J., Seeber, L. and Molnar, P., 1984, Focal depths and fault plane solutions of earthquakes and active tectonics of the Himalaya. *J. Geophys. Res.* **89**, 6918-6928.

Bilham, R.K., Larson, J. and Freymueller, P., 1997, GPS measurements of present-day convergence across the Nepal Himalaya. *Nature,* **386**, 61-64

Bott, M.H.P. and Stern, T.A., 1992, Finite element analysis of Transantarctic Mountain uplift and weval subsidence in the Ross Embayment. *Tectonophysics,* **201**, 341-356.

Burchfiel, B.C., Zhiliang, C., Hohges, K.V., Yunping, L., Royden, L.H., Changrong, D. and Jiene, X., 1992, The south Tibetan detachment system, Himalayan orogen : Extension contemporaneous with and parallel to shortening in a collisional mountain belt. *Geol. Soc. Amer., Spec, Pub.,* **269**, 41.

Burg, J.P. and Chen, G.M., 1984, Tectonics and structural zonation of southern Tibet, China. *Nature,* **311**, 219-223.

Cattin, R. and Avouac, J.P., 2000, Modeling mountain building and the seismic cycle in the Himalaya of Nepal. *J. Geophys. Res.* **105** (B6), 13389-13407.

Chandra, U., 1978, Seismicity, earthquake mechanisms, and tectonics along the Himalayan moun-

tain range and vicinity. *Phys. Earth Planet. Inter.*, **16**, 109-131.

Chen, W.P. and Molnar, P., 1977, Seismic moments of major earthquake and the average rate of slip in central Asia. *J. Geophys. Res.*, **82**, 2945-2969.

Dewey, J.F. and Bird, J.M., 1970, Mountain belts and the new global tectonics. *J. Geophys. Res.*, **75**, 2625-2647.

England, P. and Houseman, G., 1985, Role of lithospheric strength heterogeneities in the tectonics of Tibet and neighboring regions. *Nature*, **315**, 297-301.

England, P. and Houseman, G., 1986, Finite strain calculations of continental deformation, 2, comparison with the India-Asia collision zone. *J. Geophys. Res.*, **91**, 3664-3676.

England, P. and Mckenzie, D., 1982, A thin viscous sheet model for continental deformation. *Geophys. J.R. Astr. Soc.*, **70**, 295-321.

Fitch, T.J., 1970, Earthquake mechanisms in the Himalaya, Burmese and Andaman regions and continental tectonics in Central Asia. *J. Geophys. Res.*, **75**, 2699-2709.

Ganseer, A., 1964, Geology of the Himalayas. *Interscience*, London 289 p.

Ganseer, A., 1966, The Indian Ocean and the Himalayas : a geological interpretation, *Eclog. Geol. Helv.*, **59**, 831-848.

Ghose, R., Yoshika, S. and Oike, K., 1990, Three-dimensional numerical simulation of the subduction dynamics in the Sanda arc region, Southeast Asia. *Tectonophysics*, **181**, 223-255.

Golombeck, M.P., 1985, Fault type predictions from stress distributions of planetary surface : Important of fault initiation depth. *J. Geophys. Res.*, **90**, 3065-3074.

Hashimoto, S., Ohta, Y., and Akiba, C. (Editors), 1973, Geology of the Nepal Himalayas. *Saikon Publishing Co., Tokyo*, 286 pp.

Hayashi, D., 1987, Numerical simulation of the uplift of the Tibetan Plateau. *Jour. Geol. Soc. Jap.*, **93**, 587-595.

Hayashi, D. and Kizaki, K., 1972, Numerical analysis on migmatite dome with special reference to the finite element method. *Jour. Geol. Soc. Jap.*, **78** (12), 677-686.

Hayashi, D. and Talbot, C., 1992, Numerical simulation of a Himalayan profile. *Essays in Geology, Professor Hisao Nakagawa Commemorative Volume*, 53-63.

Ichikawa, M., Srivastava, H.N. and Drakopoulos, J., 1972, Focal mechanism of earthquakes occuring in and around Himalayan and Burmese mountain belt. *Papers in Meteorology and Geophysics (Tokyo)*, **23**, 149-162.

Kaneko, Y., 1995, Thermal structure in the Annapurna region, central Nepal Himalaya : implication for the inverted metamorphism. *Jour. Mineral. Petrol. Econ. Geol.*, **90**, 143-154.

Kaneko, Y., 1997, Two-step exhumation model of the Himalayan Metamorphic Belt, central Nepal. *Jour. Geol. Soc. Japan*, **103**, 203-226.

Kizaki, K., 1994, An outline of the Himalayan upheaval - a case study of the Nepal Himalayas. *JICK* (Japan International Cooperation Agency) 7-9 pp.

Lave, J. and Avouac, J.P., 1998, Active folding of fluvial terraces across the Siwaliks Hills, Himalayas of central Nepal. *J. Geophys. Res.*, **105**, 5735-5770.

Le Fort, P., 1975, Himalayas : the collided range. Present knowledge of the continental arc. *Amer. Jour. Sci.*, **275**, 1-44.

Lu, H. and Hayashi, D., 2001, Genesis of Okinawa Trough and thrust development within accretionary prism by means of 2D finite element method. *Structural Geology*, **45**, 47-64.

Lyon-Caen, H. and Molnar, P., 1985, Gravity anomalies, flexure of the Indian plate and the structure, support and evolution of the Himalaya and Ganga Basin. *Tectonics*, **4**, 513-538.

Makel, G. and Walters, J., 1993, Finite element analyses of thrust tectonics : computer simulation of detachment phase and development of thrust faults. *Tectonophysics*, **226**, 167-185.

Molnar, P., Fitch, T.J. and Wu, F.T., 1973, Fault plane solutions of shallow earthquakes contemporary tectonics of Asia. *Earth Plan. Sci. Lett.*, **16**, 101-112.

Pecher, A., 1989, The metamorphism in the central Himalaya. *Jour. Metamorphic. Geol.*, **7**, 31-41.

Peltzer, G. and Saucier, F., 1996, Present day kinematics of Asia derived from geologic fault rates. *J. Geophys. Res.*, **101**, 27943-27956.

Rastogi, B.K., 1974, Earthquake mechanisms and plate tectonics in the Himalayan region. *Tectonophysics*, **21**, 47-56.

Sakai, H., 1985, Geology of the Kali Gandaki Supergroup of the Lesser Himalaya in Nepal. *Mem. Fac. Sci., Kyushu Univ., Ser. D. Geol.*, **25**, 337-397.

Seeber, L., Armbruster, J.G. and Quittmeyer, R.C., 1981, Seismicity and Continental subduction in

the Himalayan Arc. *Geodynamics series,* **3**, 215-242.

Tandon, A.N. and Srivastava, H.N., 1975, Focal mechanisms of some recent Himalayan earthquakes and regional plate tectonics. *Bull. Seismo. Soc. Amer.,* **65**, 963-969.

Thakur, V.C., Sriram, V. and Mundepi, A.K., 2000, Seismotectonics of the great 1905 Kangra earthquake meizoseismal region in Kangra-Chamba, NW Himalaya. *Tectonophysics,* **326**, 289-298.

Timoshenko, S.P. and Goodier, J.N., 1970, Theory of Elasticity. *McGraw-Hill,* London, 3rd ed., 567 p.

Valdiya, K.S., 1980, Geology of Kumaun Lesser Himalaya. *Wadia Institute of Himalayan Geology, Dehra Dun, India,* 291 p.

Valdiya, K.S., 1980, Outline of the structure of Kumaun Lesser Himalaya. *In* Tectonic geology of the Himalaya ed., *Today and Tomorrow Pub., New Delhi,* 1-14.

Warsi, W.E.K. and Molnar, P., 1977, Plate tectonics and gravity anomalies in India and the Himalaya. *Science de la Terre, Centre National de la Recherche Scientique,* Paris, **268**, 463-478.

Widely, B.F., 1984, The evolving continents. 2nd ed. *John Wiley and Sons, Inc.,* 399 p.

Widely, B.F., 1995, The evolving continents. 3rd ed. *John Wiley and Sons, Inc.,* 526 p.

Yates, R.S. and Thakur, V.C., 1998, Reassessment of earthquake hazard based on a fault-bend fold model of the Himalayan plate-boundary fault. *Curr. Sci.* **74**, 230-233.